frontiers | Frontiers in Membrane Science and Technology

TYPE Original Research
PUBLISHED 19 September 2025
DOI 10.3389/frmst.2025.1653220



OPEN ACCESS

EDITED BY
Abdoulaye Doucouré,
Donyatek, Strategic Planning and Professional Development, United States

REVIEWED BY
Sandip Pal,
Lohum Cleantech Private Limited, India
Xiaoquan Feng,
Zhengzhou University, China

*CORRESPONDENCE
Mihail Barboiu,
mihail-dumitru.barboiu@umontpellier.fr

RECEIVED 24 June 2025
ACCEPTED 22 August 2025
PUBLISHED 19 September 2025

CITATION
Yahia M, Neves LA, Giorno L, Crespo J and Barboiu M (2025) Polyethylene oxide rubbery organic framework (ROF) membranes with enhanced $CO_2$ permeability and $CO_2$/$CH_4$ selectivity.
*Front. Membr. Sci. Technol.* 4:1653220.
doi: 10.3389/frmst.2025.1653220



# Polyethylene oxide rubbery organic framework (ROF) membranes with enhanced $CO_2$ permeability and $CO_2/CH_4$ selectivity

Mohamed Yahia[1,2], Luísa A. Neves[3], Lidietta Giorno[4], João Crespo[3] and Mihail Barboiu[5,6]*

[1]Chemistry Department, Faculty of Science, Helwan University, Cairo, Egypt, [2]Center for Cooperative Research on Alternative Energies (CIC energiGUNE), Basque Research and Technology Alliance (BRTA), Vitoria-Gasteiz, Spain, [3]LAQV@REQUIMTE, Department of Chemistry, NOVA School of Science and Technology, Universidade NOVA de Lisboa, Campus da Caparica, Caparica, Portugal, [4]Institute on Membrane Technology, ITM-CNR, University of Calabria, Cosenza, Italy, [5]Adaptative Supramolecular Nanosystems Group, Institut Européen des Membranes, ENSCM/UMII/UMR-CNRS 5635, Montpellier, France, [6]Babes-Bolyai University, Supramolecular Organic and Organometallic Chemistry Center (SOOMCC), Cluj-Napoca, Romania

Rubbery organic frameworks (ROFs), assembled *via* reversible covalent bonds under dynamic molecular control, represent a promising class of adaptive polymers for gas separation membranes. Elastomeric ROF membranes exhibit excellent mechanical stability, dynamic responsiveness, and intrinsic microporosity. Their affinity for carbon dioxide ($CO_2$) enables both high $CO_2$ permeability and enhanced selectivity compared to conventional glassy polymeric membranes. One effective strategy for improving $CO_2$ separation performance is the incorporation of polyethylene oxide (PEO) units into the ROF structure. Owing to the high $CO_2$ solubility and electrostatic interactions with PEO segments, this approach can significantly boost $CO_2$ selectivity over other gases such as methane ($CH_4$). In this study, a new class of PEO-based ROF membranes were developed and tailored by varying the length of PEO segments to optimize both mechanical strength and $CO_2/CH_4$ separation performance. The membranes were systematically characterized to understand the relationship between their molecular architecture, morphology, and gas transport properties. The resulting ROF membranes demonstrated $CO_2$ permeabilities ranging from 155 to 180 barrer and $CO_2/CH_4$ selectivities between 15 and 31. Notably, a synergistic enhancement in both $CO_2$ permeability and selectivity was observed with increasing PEO segment length. This improvement is attributed to a favorable balance of polymer chain packing, diffusivity, and $CO_2$ affinity within the membrane matrix. These findings highlight the potential of PEO-integrated ROFs as versatile and high-performance materials for advanced gas separation applications.

KEYWORDS

**rubbery organic frameworks, dynameric membranes, $CO_2/CH_4$ separation, polyethylene oxide, membranes**

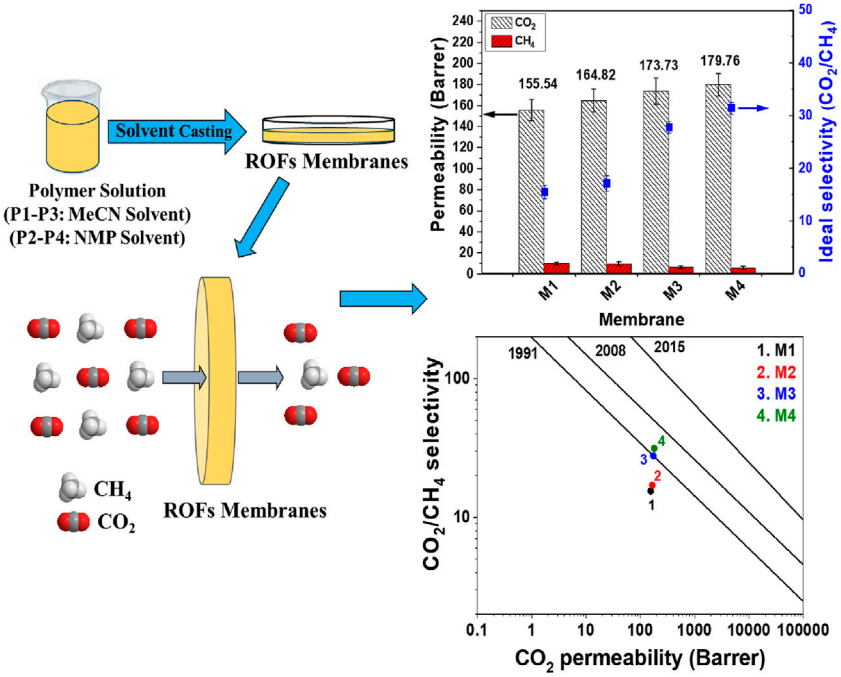


GRAPHICAL ABSTRACT

## 1 Introduction

In the last decade, membrane technology based on polymeric materials has received great attention in gas separation applications, offering numerous eco-friendly and cost-effective benefits over conventional separation processes such as sorption–desorption and cryogenic distillation (Brunetti et al., 2010) due to notable advantages such as simple design and scale-up and energy saving (Alexander Stern, 1994; Budd et al., 2005; Basu et al., 2010; D'Alessandro et al., 2010; Reijerkerk et al., 2010; Yave et al., 2010; Zou and Zhu, 2018; McKeown, 2020). Furthermore, membrane-based processes offer low capital and operating costs, design flexibility and consistent performance and are suitable for remote areas. Most significantly, they eliminate the need for phase changes or thermal forces, which can reduce energy consumption by up to 90% compared to conventional thermal separation methods (Corrado and Guo, 2020). However, the primary goal in developing gas separation membranes is to achieve both high permeability and adequate selectivity, which is typically limited by the well-known trade-off between these two properties (Robeson, 1991; Freeman, 1999; Robeson et al., 2009; Swaidan et al., 2015; Comesaña-Gándara et al., 2019).

Despite efforts to produce novel polymeric membranes for gas separation processes that can overcome the limitations of commercial membranes and compete with current separation technologies, only a few conventional polymeric materials are in use (Wang et al., 2016). Recently, both commercial and exploratory polymeric membranes were both reported for pair gas separation ($CO_2/CH_4$) (Freeman, 1999; Robeson et al., 2009; Corrado and Guo, 2020; Refaat et al., 2024; Yahia et al., 2024; Yahia et al., 2025). However, these membranes often exhibit either high permeability with low selectivity or vice versa (Staudt-Bickel and J. Koros, 1999; Pourafshari Chenar et al., 2006), significantly limiting their scalability and practical application. Most membranes are made from glassy or rubbery polymers. To overcome these challenges, a recent class of composite membranes, known as mixed matrix membranes (MMMs), were developed that combine the advantages of polymer material flexibility and high selectively porous materials such as metal organic frameworks (MOFs) and zeolites (ZIFs) (Aroon et al., 2010; Denny et al., 2016; Koros and Zhang, 2017; Chuah et al., 2018; Refaat et al., 2024; Yahia et al., 2024; Yahia et al., 2025). This has led to a synergistic approach of improving membrane selectivity and permeability to surpass upper-bound correlations (Swaidan et al., 2015; Comesaña-Gándara et al., 2019). Recently, polyethylene oxide (PEO)-based polymers have shown promising potential for separating $CO_2$ from $CH_4$, owing to the strong adsorption affinity between $CO_2$ and ether oxygen atoms. Such polymers were fabricated via UV irradiation as cross-linked polymer membranes, demonstrating good performance for $CO_2/CH_4$ separation (Patel et al., 2004; Lin et al., 2006a; Lin et al., 2006b). Nevertheless, these systems face several drawbacks, such as difficulty in large-scale fabrication, inhomogeneity, film defects, high crystallinity, limited mechanical strength, and high operating costs, restricting their industrial applicability (Xing and Ho, 2009). Different design strategies have been applied to solve these issues, such as copolymerization, crosslinking, and physical blending with other polymers (polyethylene glycol–PEG or polyimides) to generate permeable PEO-based membranes for $CO_2$ separation with controlled physical properties based on PEO molecular weight or unit length (Car et al., 2008; Petzetakis et al., 2015; Ioannidi et al., 2021). Moreover, membrane microstructure design and control over fractional free volume (FFV) have

become critical topics in enhancing $CO_2$ separation performance (Wang et al., 2016). Therefore, several studies have investigated PEO-based membranes or membrane containing polar ether groups that can interact with acidic $CO_2$ to improve $CO_2$ separation performance (Kawakami et al., 1982; Li et al., 1995; Okamoto et al., 1995; Chatterjee et al., 1997; Suzuki et al., 1998; Bondar et al., 2000; Yoshino et al., 2000; Kim et al., 2001; Sanchez et al., 2002; Lin and Freeman, 2004).

"Dynameric membranes" refer to membranes constructed from dynamic polymers (dynamers), which are formed via reversible covalent bonds (Barboiu, 2013). These bonds allow the polymer network to undergo self-healing, reconfiguration or adaptive behavior in response to external stimuli (e.g., heat, solvents, and pH). In membrane science, such dynamic covalent frameworks provide tunability, defect correction, and potential recyclability, offering advantages over traditional static polymeric membranes. Rubbery organic framework (ROF) membranes are among the most well-known types of dynamers. Our group has recently pioneered their development for gas separation applications (Nasr et al., 2012; Zhang and Barboiu, 2016; Dupuis et al., 2022).

ROFs are formed through dynamic molecular control using reversible covalent bonds between core centers and flexible connectors, resulting in mechanically stable membranes with high permeability and enhanced selectivity compared to traditional polymeric membranes (Nasr et al., 2008; Roy et al., 2015; Dupuis et al., 2022; Sandru et al., 2024). Their structure is controlled at the molecular level, offering exceptional flexibility, mechanical stability, and guest-responsiveness. This innovative strategy opens new avenues for creating adaptive membranes with excellent gas transport performance (Nasr et al., 2008; Roy et al., 2015; Dupuis et al., 2022). Additionally, the wide variety of available building blocks with diverse shapes and chemical structures allows for unlimited design flexibility, giving ROFs high tunability for specific gas separations (Nasr et al., 2012; Zhang and Barboiu, 2016; Dupuis et al., 2022). Furthermore, they represent a promising class of dynamic polymers that differ fundamentally from conventional crystalline frameworks such as metal–organic frameworks (MOFs) and covalent organic frameworks (COFs). While MOFs and COFs rely on rigid and ordered architectures, ROFs are constructed via reversible covalent bonding (e.g., imine, hydrazone or boronate ester linkages) that affords an amorphous, elastomeric structure with inherent flexibility. This dynamic network enables ROFs to present a segmental chain mobility, leading to a unique balance of high gas permeability and selectivity, by avoiding the high cross-linking behaviors due to excessive segmental mobility. One of the key advantages of ROFs is their ability to form free-standing, flexible membrane films without requiring blending with other polymers, in contrast with MOFs and COFs that are commonly used as fillers in mixed-matrix membranes (MMMs) or as thin layers on supports. Moreover, the rubbery nature of ROFs contributes to good processability, thermal stability, and mechanical resilience—essential features for practical membrane fabrication and operation under variable conditions (Zhang and Barboiu, 2016; Kang et al., 2023; Sandru et al., 2024). These characteristics position ROFs as a versatile and scalable platform for gas separation applications, particularly for $CO_2$ capture and light gas separation where membrane flexibility, high throughput, and selective transport are critical.

Our study aims to construct economically and technically viable ROF membranes incorporating polyethylene oxide (PEO) segments for $CO_2/CH_4$ separation. To achieve optimal mechanical strength and gas separation performance, the membrane architecture was tailored and controlled using different solvents and PEO-based monomers during the polymerization reaction. Four PEO-based ROF membranes were fabricated via imine chemistry, involving a benzene-1,3,5-tricarbaldehyde core and PEO-diamine segments containing ethylene oxide chains of varying lengths. The membranes were structurally characterized to evaluate their chemical structure, thermal stability, and morphology. Their single gas separation performance was tested for $CO_2/CH_4$ separation, and the results were benchmarked against previously reported membranes (Luo et al., 2016; Azizi et al., 2017; Bandehali et al., 2020) and positioned on the Robeson upper bound plots (Robeson, 1991; Freeman, 1999; Robeson, 2008; Robeson et al., 2009; Rowe et al., 2010; Swaidan et al., 2015; Comesaña-Gándara et al., 2019).

# 2 Materials and methods

## 2.1 Materials

For synthesizing ROFs, benzene-1,3,5–tricarbaldehyde— 2,2′-(Ethylenedioxy)bis(ethylamine) or 4,7,10-trioxa-1,13-tridecanediamine—acetonitrile (MeCN), and N-methyl-2-pyrrolidone (NMP) were used. All reagents were purchased from Sigma-Aldrich and used without further purification (purity ≥98%).

## 2.2 Polymer synthesis and membrane fabrication

Four polymeric materials (P1–P4) were synthesized and used to fabricate the corresponding membranes (M1–M4). Each polymer was obtained via an imine-condensation reaction between benzen-1,3,5-tricarbaldehyde core centers and one of 2,2′-(Ethylenedioxy) bis(ethylamine) or 4,7,10-trioxa-1,13-tridecanediamine segments. Polymers P1 and P2 were prepared using the former, while P3 and P4 were synthesized using the latter with an aldehyde-to-diamine molar ratio of 1:1.5. MeCN was used as the solvent for P1 and P3, while NMP was used for P2 and P4. The resulting polymer solutions were transferred into 100-mL round-bottom flasks and refluxed at 70 °C with continuous stirring overnight. The chemical structures of the reaction units used to synthesize the four polymers are presented in Supplementary Figure S1.

After polymerization, membranes M1–M4 were obtained by casting the corresponding polymer solutions (P1–P4) onto Teflon plates, followed by slow solvent evaporation and drying under vacuum at 80 °C overnight. The choice of MeCN and NMP as solvents for ROF synthesis was based on their polar aprotic nature, which supports reversible imine bond formation and ensures good solubility of all monomers. Moreover, their distinct boiling points and polarity profiles influence membrane morphology: MeCN promotes faster evaporation and denser structures, while NMP allows more reaction time, probably leading to an open network formation due to slower solvent removal. These differences impact

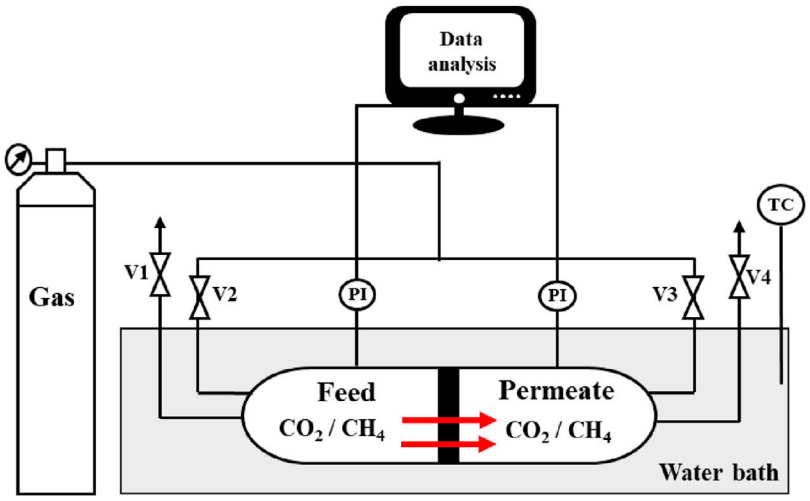


FIGURE 1
Experimental setup for single gas permeability measurements (Neves et al., 2012; Abdelrahim et al., 2017).

the microstructure and, ultimately, the gas separation performance of the resulting membranes.

## 2.3 Membrane characterization

The physicochemical properties of fabricated ROF membranes were characterized before gas permeability testing. The chemical structures were confirmed by $^1$H NMR (BRUKER NMR AVANCE 300 MHz) and FTIR spectroscopy (Nicolet 710). Thermal stability was assessed via thermogravimetric analysis (TGA, Hi-Res TGA 2950, TA Instruments) and differential scanning calorimetry (DSC, Modulated DSC 2920, TA Instruments). The thickness and quality of the cast membranes were examined using scanning electron microscopy (SEM, Hitachi S-4800 field emission microscope). A digital micrometer was used to manually measure the membrane thickness at five different points. The average value and standard deviation were calculated to ensure accuracy and account for variability. The contact angle was measured using ImageJ software to provide insights into the membrane surface properties, particularly hydrophobicity.

## 2.4 Membrane permeability measurements

Single gas permeability measurements for $CO_2$ and $CH_4$ gases with purity (99.99%) were carried out at 30 °C using the experimental setup shown in Figure 1. The setup was composed of two identical compartments (feed and permeate) made of stainless steel, which were separated by the membrane to be tested with an effective surface area of 9.62 cm$^2$. The desired pure gas was pressurized through both compartments (feed and permeate) and a pressure difference (~0.7 bar) was imposed after opening the permeate outlet. Two pressure transducers (Druck, PDCR 910 models 99166 and 991675, England) were used to monitor the pressure profiles in each compartment. An Elcometer® 124 Thickness Gauge (United Kingdom) instrument was used to estimate the membrane thickness.

### 2.4.1 Permeability and $CO_2/CH_4$ ideal selectivity

The single gas permeabilities through the fabricated membranes were calculated from the pressure data recorded from the feed and permeate compartments (Figure 1) according to Equation 1 (Cussler, 2009):

$$\frac{1}{\beta}\ln\left(\frac{\left[P_{feed}-P_{perm}\right]_0}{\left[P_{feed}-P_{perm}\right]}\right)=P\frac{t}{l} \quad (1)$$

—where feed ($P_{feed}$) and permeate pressure ($P_{perm}$) are in (bar), membrane permeability (P) is in (m$^2$/s), membrane thickness (l) in (m), time (t) in (s), and the parameter characteristic of the cell geometry (β) in (m$^{-1}$) are calculated as per Equation 2 (Cussler, 2009).

$$\beta = A\left(\frac{1}{V_{feed}}+\frac{1}{V_{perm}}\right) \quad (2)$$

—where membrane area (A) is in (m$^2$) and the feed ($V_{feed}$) and permeate volume ($V_{perm}$) of compartments are in (m$^3$). Gas permeability is represented as the slope from the data plotted as $[\ \frac{1}{\beta}\ln(\frac{\Delta P_0}{\Delta P})$ versus $\frac{t}{l}\ ]$, and ideal selectivity ($\alpha_{A/B}$) is calculated by dividing the permeabilities of two different pure gases (A and B) as per Equation 3:

$$\alpha_{A/B}=\frac{P_A}{P_B} \quad (3)$$

Each gas permeability measurement was repeated three times for each membrane sample to ensure consistency. The recorded permeability values represent the average of three independent measurements, and the ±values indicate the standard deviation (Supplementary Figure S1).

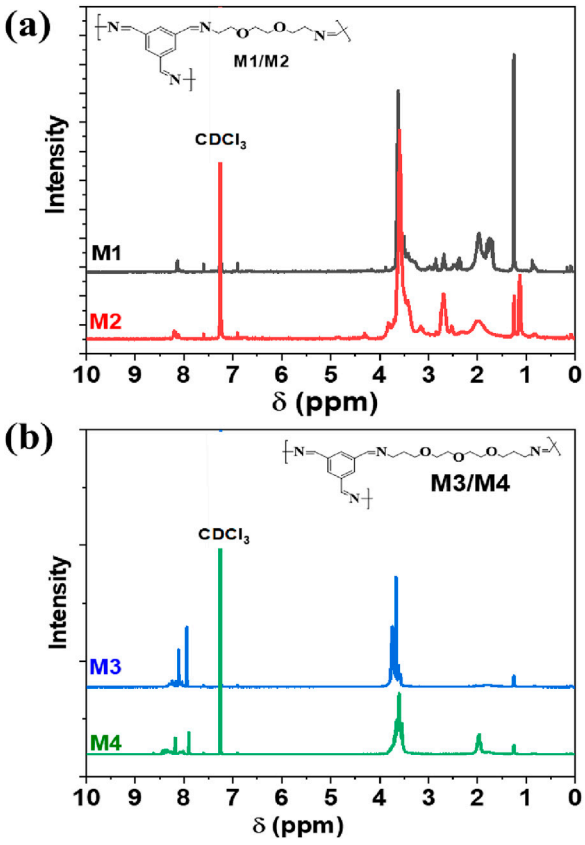


FIGURE 2
$^{1}$HNMR spectra for the synthesized polymers **(a)** M1/M2 and **(b)** M3/M4.

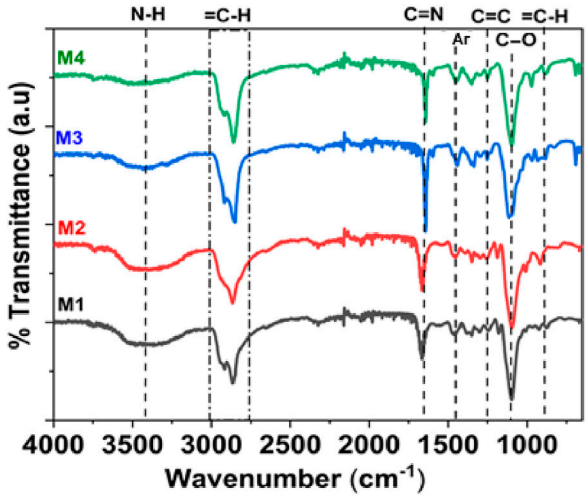


FIGURE 3
FTIR spectra for the fabricated polymeric membranes.

# 3 Results and discussion

## 3.1 Proton nuclear magnetic resonance ($^{1}$H NMR)

The $^{1}$H-NMR spectra for the synthesized polymers were recorded in deuterated chloroform ($CDCl_3$) at 300 MHz (Figures 2a,b). The spectra in Figure 2 indicate the presence of signals at 8.5–8 ppm, which are associated with the formed imine bond formation (PEO–NCH) within the polymer matrix. The signals around 8.0–7.5 ppm correspond to the aromatic benzene rings, while those at the aliphatic region (4.0–1.0 ppm) correspond to the methylene (–$CH_2$–) protons of PEGs groups (Vöge et al., 2014b; Abdelrahim et al., 2016).

## 3.2 Fourier transformed infrared (FTIR)

Figure 3 shows the FTIR spectra of the synthesized ROF membranes, confirming the formation of imine bonds. The peaks at 1,661.3 cm$^{-1}$ correspond to C=N stretching mode for imine groups within the polymer structure, while the peak of aldehyde groups observed at 1700 cm$^{-1}$ disappear (Abdelrahim et al., 2016; Ioannidi et al., 2021). The peaks at 2,926.4 cm$^{-1}$ and 874.5 are respectively associated with C–H stretching and bending modes for aliphatic PEO (Luo et al., 2016; Vollas et al., 2018). The peaks at 2,871.6 cm$^{-1}$ and 1,097.0 cm$^{-1}$ are respectively attributed to C–H (aliphatic) stretching and bending modes (Abdelrahim et al., 2016; Ioannidi et al., 2021). The peaks at 1,447.3 cm$^{-1}$ and 1,254.5 cm$^{-1}$ are respectively linked to the C=C stretching mode of aromatic ring and C–O ether bonds (Vöge et al., 2014a; Luo et al., 2016; Ioannidi et al., 2021).

## 3.3 Thermal TGA and DSC analysis

Figure 4a shows the TGA measurements for the fabricated membranes. The polymeric samples were preheated at 100 °C for 30 min under nitrogen flow (10 °C/min) to remove the adsorbed water within the polymer matrix. The degradation curves were recorded in a nitrogen flow (10 °C/min) to a maximum heating temperature (700 °C). It was observed that there are two stages of thermal degradation for all membranes. The first degradation stage had a mass loss of ~10 wt% for M1 and M2 at 100 °C–175 °C and a mass loss of ~5 wt% for M3 and M4 at 100 °C–250 °C.

This first degradation stage is attributed to the evaporation of moisture and residual solvent present within the polymer's backbone. The second degradation stage shows a mass loss of ~95 wt% for M1 and M2 occurring between 175 °C and 450 °C, while for M3 and M4, a similar mass loss of ~95 wt% occurred between 250 °C and 700 °C. This degradation stage should be ascribed to the thermal decomposition and loss of polyethylene oxide (PEO) chains within the membrane structure (Fares et al., 1994; Theodosopoulos et al., 2017; Ioannidi et al., 2021). The main decomposition products were non-cyclic ethers (i.e., ethoxy-ethane and methoxy-methane), ethylene oxide, $CO_2$, CO, and water (Fares et al., 1994; Theodosopoulos et al., 2017; Ioannidi et al., 2021).

The two stages in the figure demonstrate that higher temperatures are required for thermal degradation in membranes with longer PEO chains (M3 and M4) than those with shorter PEO chains (M1 and M2). This indicates that the thermal stability of M3 and M4 is higher than that of M1 and M2 owing to the presence

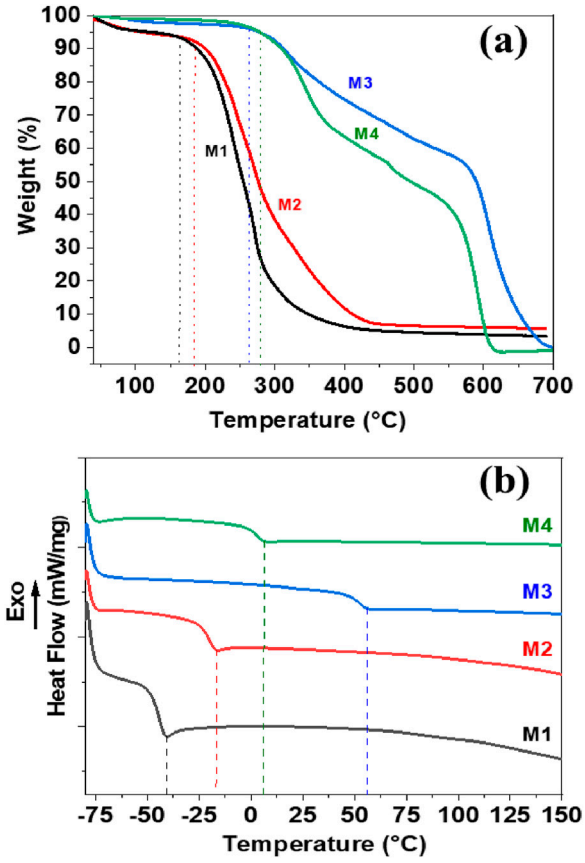


FIGURE 4
Thermal stability measurements for the fabricated membranes: **(a)** TGA and **(b)** DSC.

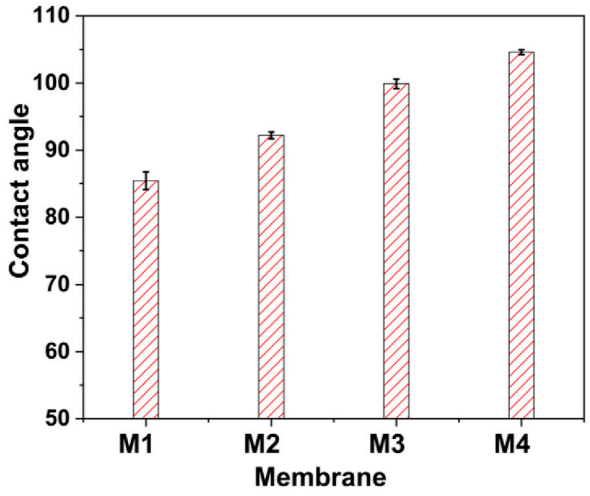


FIGURE 5
Contact angle measurements for the fabricated membranes M1-M4.

of longer PEO chains. These enhance the degree of crystallinity within the membrane structures, as previously observed in other PEO-based membranes, where crystallinity increased with the length of the PEO backbone (Theodosopoulos et al., 2017; Ioannidi et al., 2021; Sandru et al., 2024).

Figure 4b shows the differential scanning calorimetry (DSC) measurements for the fabricated membranes. The measurements were performed under nitrogen flow (10 °C/min) up to a maximum heating temperature of 150 °C. As shown in the figure, the recorded glass transition temperatures (Tg) are approximately −45, −20, 5, and 50 °C for M1, M2, M3, and M4, respectively. This means that membranes M3 and M4 with longer PEO chains exhibit higher Tg values than M1 and M2, which have shorter PEO chains. As mentioned before, this might be related to the crystallization behavior of longer PEO chains within the polymer matrix, which enhances the potential for higher crosslinking through the membrane's backbone. Furthermore, higher Tg values indicate restricted segmental motion and a more rigid ROF network, which tends to reduce chain packing defects and enhance size-sieving. This results in improved selectivity, especially for gas pairs with small differences in kinetic diameter, such as $CO_2$ and $CH_4$ with kinetic diameters of approximately 3.3 Å and 3.8 Å, respectively (Robeson, 2008; Robeson et al., 2009). Therefore, ROF membranes with higher PEO content are expected to achieve slightly increased Tg and corresponding improvements in $CO_2/CH_4$ selectivity, consistent with this mechanism.

## 3.4 Contact angle measurements

Figure 5 and Supplementary Figure S2 represent the contact angle values obtained for the fabricated ROF membranes. The measurements were recorded using the ImageJ contact angle plugin, a widely used image analysis tool for quantifying the wettability of surfaces by measuring the contact angle formed between a liquid droplet and a solid substrate. The analysis provides an accurate and reproducible estimation of surface hydrophilicity or hydrophobicity. In this study, water droplets were placed on the membrane surface, images were captured with a calibrated camera, and three measurements per sample were averaged to ensure reliability and minimize error due to surface heterogeneity (Giovambattista et al., 2007).

As shown in Figure 5 and Supplementary Figure S2, the reported contact angle values represent the average of the observed left- and right-angle measurements, which were nearly identical. The relatively high contact angles suggest that the fabricated membranes possess high hydrophobicity and a symmetrical surface morphology. Moreover, Figure 5 shows that the recorded contact angles for membranes with longer PEO chains (M3 and M4) are slightly higher than those for membranes with shorter PEO chains (M1 and M2). This means that M3 and M4 exhibited higher hydrophobic surface properties than M1 and M2, owing to the higher crosslinking degree within the M3 and M4 membrane backbones.

Furthermore, the figure showed that the synthesized membranes demonstrate this trend consistently. This is a surprising observation, showing the solvent effect on the polymerization and crosslinking properties of the fabricated polymeric membranes, as it results in variations in the chemical, crosslinking, and hydrophobic properties of the developed membranes. In addition, the contact angle measurements obtained agree with the data from the thermal

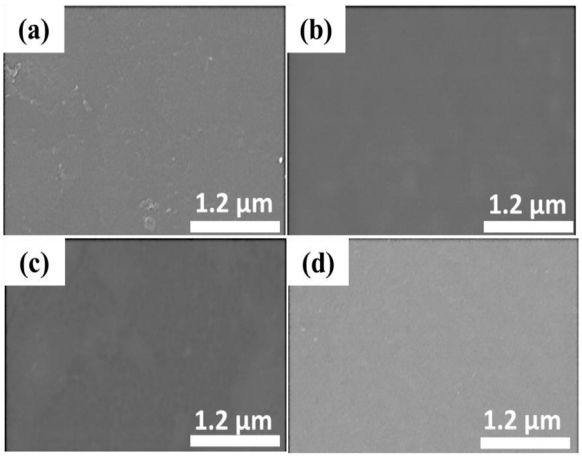


FIGURE 6
SEM images for the fabricated membranes: surface views for M1 **(a)**. M2 **(b)**. M3 **(c)**. M4 **(d)**.

analysis measurements: membranes synthesized in NMP solvent (M2 and M4) exhibited slightly higher thermal degradation stability and glass transition temperatures than those synthesized in MeCN solvent (M1 and M3, respectively) under similar polymerization conditions.

The organic solvent enhances the mobility of the building units, increasing the likelihood of the reactive groups approaching each other to initiate polymer bond formation (HC = N). Additionally, the NMP solvent interacts more strongly with the PEO segments, removing water from interactions with the PEO chains and therefore controlling the structural organization of the ROF materials; this affects their pore distribution and fractional pore volume within the membrane backbones. Therefore, the utilization of organic solvents with different polarities in the polymerization reaction affects the chemical structure of the fabricated ROF membranes, as previously observed in molecular simulation studies (Dupuis et al., 2022).

## 3.5 Scanning electron microscopy (SEM)

Figures 6, 7 present the SEM images of the fabricated polymeric membranes, displaying both surface and cross-section views, respectively. The SEM images reveal that the membranes exhibit a dense and nonporous structure. The thickness of the membranes was consistently approximately 300 ± 25 µm, indicating uniformity in membrane fabrication. Additionally, no visible pores or defects were observed on the membrane surface, confirming its compact nature. The recorded thicknesses agree with our previous findings (Abdelrahim et al., 2016; Sandru et al., 2024), and were chosen based on our prior experience with ROF membranes to balance mechanical stability, ease of handling, and reproducible casting. A uniform thickness is critical for minimizing defect formation during solvent evaporation. While permeance is inversely proportional to membrane thickness, selectivity remains largely unaffected as it depends on the ratio of gas permeabilities. This behavior is consistent with the solution–diffusion transport mechanism typical for dense and hybrid polymer membranes. Furthermore, Figure 7 shows that M1 and M2 display homogeneous monolithic profiles, whereas M3 and M4 reveal faint lamellar features near the edges, attributable to PEO-induced phase separation. These minor differences in surface texture and layer uniformity align with variations in solvent evaporation rates and polymer PEO segment mobility, which are critical for tailoring membrane properties.

## 3.6 Flexibility and mechanical measurements

The flexibility and manual mechanical test for the fabricated ROF membranes was performed by us previously (Sandru et al., 2024). As shown in Supplementary Figure S3, the ROF membrane exhibited good flexibility and mechanical integrity upon manual bending and folding. No visible cracks, delamination or structural damage were observed, indicating that the ROF membrane possesses sufficient mechanical robustness for handling and potential gas separation applications.

## 3.7 Gas permeabilities and ideal selectivities

The pure gas permeabilities through the fabricated membranes (M1–M4) and the ideal selectivities for the pure gases $CO_2$ and $CH_4$ were determined at 30 °C under a pressure difference of 0.7 bar (Supplementary Table S1). The results show that, for all membranes, $CO_2$ permeability is higher than $CH_4$ permeability. This behavior is attributed to specific parameters such as the dipolar interactions of $CO_2$ molecules with the imine (–HC = N) and PEO functional groups within the ROF membranes, as well as the higher polarity and quadrupole moment of $CO_2$ in comparison with the nonpolar $CH_4$ gas. Moreover, the kinetic diameter of $CO_2$ is smaller than that of $CH_4$, which facilitates its diffusion. These factors collectively influence $CO_2$ adsorption affinity and diffusion through the fabricated membranes (Bao et al., 2011; Basu et al., 2011; Herm et al., 2011; Nordin et al., 2015; Yahia et al., 2024; Yahia et al., 2025). Furthermore, $CO_2$ permeability through the M3 and M4 membranes was higher than that of M1 and M2, indicating the influence of membrane composition on gas transport properties. This might be related to the higher hydrophobic surface and higher glass transition properties of M3 and M4 compared to M1 and M2 owing to the differences in the PEO chains within the membrane's backbones. As mentioned previously, M3 and M4 possess longer PEO chains, and this might cause an increase in the fractional free volume (FFV) and enhance $CO_2$ diffusion through the membrane chains. Furthermore, the membranes synthesized in NMP solvent showed higher permeability values and selectivity than those synthesized in the MeCN solvent. This behavior could be attributed to the solvent's effect on the membrane's chemical structure and crosslinking degree, as mentioned in Sections 3.3 and 3.4.

Figure 8 shows the relationship between the permeability ($PCO_2$) and ideal selectivity ($CO_2/CH_4$) for the fabricated membranes. Results show that the ideal selectivity for membranes fabricated with shorter PEO chains is higher than for

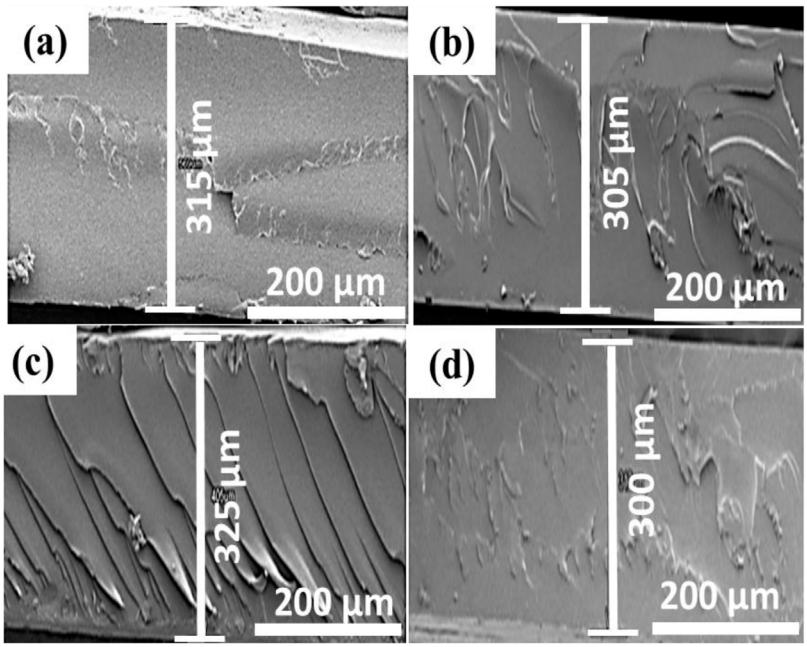


FIGURE 7
SEM images for the fabricated membranes: cross-section views for M1 **(a)**. M2 **(b)**. M3 **(c)**. M4 **(d)**.

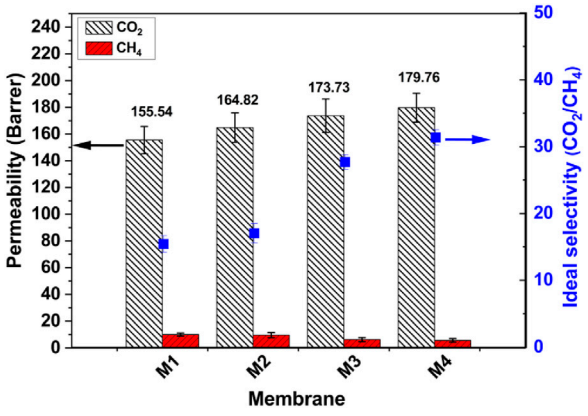


FIGURE 8
Gas separation performance as a relationship between $CO_2$ and $CH_4$ permeabilities and ideal selectivity ($CO_2/CH_4$) for the fabricated membranes (M1-M4).

membranes fabricated with longer PEO chains. This indicates that the presence of longer PEO chains within the membrane structure slightly increases both $CO_2$ permeability and ideal selectivity. It is worth noting that both $CO_2$ permeability and ideal selectivity increase simultaneously, which is uncommon (Robeson, 1991; Freeman, 1999; Robeson, 2008; Robeson et al., 2009; Swaidan et al., 2015; Comesaña-Gándara et al., 2019; Corrado and Guo, 2020). This indicates that replacing short-chain functional groups with longer-chain groups within the membrane structure improves membrane performance. Therefore, the incorporation of longer polyethylene oxide (PEO) chains and NMP solvent into the membrane matrix was expected to enhance $CO_2$ permeability over $CH_4$. This effect is attributed to structural changes in the membrane and enhanced affinity toward $CO_2$ (Dupuis et al., 2022; Sandru et al., 2024).

Furthermore, the kinetic diameters of $CO_2$ and $CH_4$ are approximately 3.3 Å and 3.8 Å, respectively (Robeson, 2008; Robeson et al., 2009). This difference plays a critical role in their transport through the membrane. In polymeric and hybrid membranes such as ROF-based MMMs, gas separation occurs predominantly via the solution–diffusion mechanism, where permeability is a function of both diffusivity and solubility. The smaller size of $CO_2$ allows it to diffuse more easily through the membrane matrix, while its higher condensability and quadrupole moment enable stronger interactions with polar groups such as ether oxygens in PEO and imine functionalities (–HC = N) within the ROF framework (Fares et al., 1994; Giovambattista et al., 2007; Basu et al., 2011; Nordin et al., 2015). These interactions enhance $CO_2$ solubility via dipole-quadrupole and Lewis acid–base interactions, resulting in significantly higher $CO_2$ permeability and selectivity over $CH_4$. On the other hand, $CH_4$, being non-polar and less condensable, lacks such specific interactions and exhibits lower diffusivity due to its larger kinetic diameter. Therefore, the combination of size-exclusion effects, specific $CO_2$–polymer interactions, and the flexible as well as microporous nature of ROFs synergistically contribute to the observed superior $CO_2$/$CH_4$ separation performance.

Nevertheless, the most significant goal in gas membrane development is the combination of high permeability and acceptable selectivity, which is limited by the trade-off between permeability and selectivity. Furthermore, Figures 9a, b illustrate the $CO_2/CH_4$ separation performance of the fabricated ROF membranes (M1–M4) compared to previously reported PEO-based membranes (Supplementary Table S2—Rahman et al.,

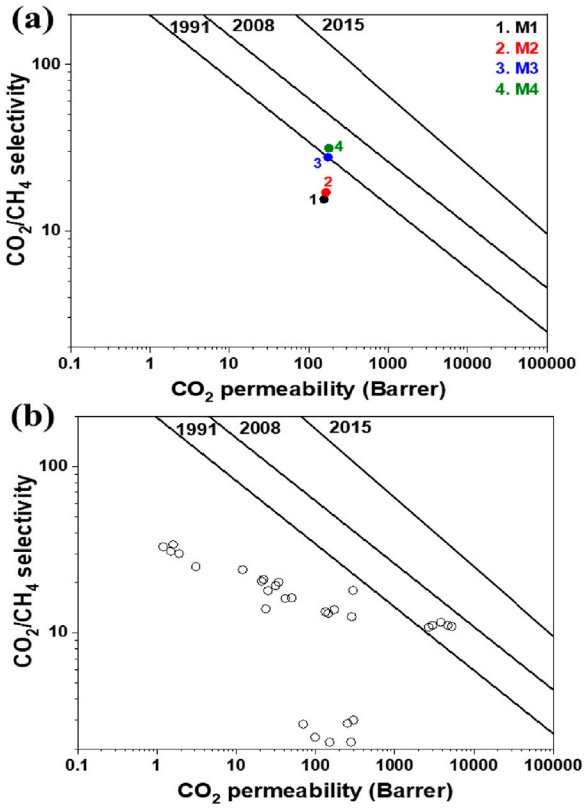


FIGURE 9
The upper-bound lines 1991 (Robeson, 1991), 2008 (Robeson, 2008), and 2015 (Swaidan et al., 2015) for **(a)** the membranes M1-M4 described in this work and for **(b)** other PEO polymeric membranes from data described in literature.

2013; Tena et al., 2013; Ghadimi et al., 2014; Qiu et al., 2016; Bengtson et al., 2017; Chen et al., 2017; Nebipasagil et al., 2017; Bandehali et al., 2020) plotted against the 1991, 2008, and 2015 Robeson upper-bound correlations (Robeson, 1991; Robeson, 2008). The $CO_2/CH_4$ selectivity is shown as a function of $CO_2$ permeability.

The reference lines represent the Robeson upper bounds, which indicate the classical trade-off between permeability and selectivity observed in most polymeric membranes. Typically, as permeability increases, selectivity decreases. In contrast to this trend, the fabricated membranes in this study (M1–M4) show a clear and steady increase in both $CO_2$ permeability and $CO_2/CH_4$ selectivity as we move from M1 to M4. Specifically, M1 and M2 lie below the 1991 Robeson upper bound, M3 lies directly on this upper bound, and M4 surpasses the 1991 limit and approaches the 2008 Robeson upper bound, thus demonstrating significant overall improvement in separation performance.

This remarkable behavior can be attributed to the tailored design of the ROF membranes through the incorporation of different PEO segment lengths and the use of organic solvents with varied polarity during the synthesis process. This strategy enhances polymer packing, dynamic mobility, and gas sorption affinity. Specifically, the increased $CO_2$ affinity of the ROF membranes (via PEO and imine groups), combined with the smaller kinetic diameter of $CO_2$ relative to $CH_4$, improves $CO_2$ transport without negatively impacting $CH_4$ transport, thus permitting performance beyond the 1991 Robeson limit and potentially enabling future designs to surpass both the 2008 (Robeson, 2008) and 2015 (Swaidan et al., 2015) upper bound limits. Hence, our findings strongly support the hypothesis that the strategic tuning of polymer architecture and processing conditions can overcome the conventional permeability–selectivity trade-off and unlock new performance frontiers for $CO_2/CH_4$ separation. This validates the promise of ROF membranes as a competitive platform for advanced gas separation applications. Furthermore, to evaluate the stability of the fabricated ROF membranes, preliminary aging tests were conducted by storing the membranes under ambient conditions for 1 month. The results showed no significant changes in gas permeability or selectivity, indicating good structural stability and resistance to physical aging over time.

As shown in Supplementary Table S3, the developed ROF membranes (M1–M4) demonstrate $CO_2$ permeability (155.54–179.76 barrer) superior to conventional polymeric membranes such as cellulose acetate (CA) (1.26–52.6 barrer) (Moghadassi et al., 2014; Sanaeepur et al., 2016; Mubashir et al., 2018; Mubashir et al., 2019; Jia et al., 2020) and Matrimid® (12–20 barrer) (Dorosti et al., 2014; Kertik et al., 2017). While some CA-based membranes achieve higher $CO_2/CH_4$ selectivity (up to 53.98—Moghadassi et al., 2014), this is typically accompanied by low $CO_2$ permeability (≤5 barrer), highlighting the permeability–selectivity trade-off common in polymeric membranes. In contrast, the synthesized membranes (M1–M4) exhibit a balanced performance, with selectivity values (15.45–31.4) comparable to or exceeding those of commercial membranes, such as CA: 4.44–53.98 (Moghadassi et al., 2014; Sanaeepur et al., 2016; Mubashir et al., 2018; Mubashir et al., 2019; Jia et al., 2020) and polyimide (P84): 67–93 (Guo et al., 2018; Sheng et al., 2020), while maintaining significantly higher gas permeation rates. Furthermore, the solvent choice (NMP or MeCN) appears to influence membrane performance, with NMP-processed membranes (M2, M4) showing marginally higher permeability and selectivity than their MeCN counterparts (M1, M3). This trend aligns with studies on conventional polymers, where solvent selection impacts membrane morphology and gas transport properties (Moghadassi et al., 2014; Sanaeepur et al., 2016; Mubashir et al., 2018; Mubashir et al., 2019; Jia et al., 2020). Notably, the performance of M3 and M4 approaches the upper bound for polymeric membranes, suggesting their potential for industrial $CO_2/CH_4$ separation applications where both high permeability and selectivity are critical.

Although single-gas permeation tests were conducted in the current study due to the limitations of our manual setup (operating up to 3 bar), these tests remain widely accepted for preliminary screening of membrane materials, offering valuable insights into intrinsic permeability and selectivity (Baker and Low, 2014). The applied conditions (30 °C, up to 3 bar with pressure difference ~0.7 bar) are also relevant to practical applications such as biogas upgrading (Sridhar et al., 2007). To complement these results, our group recently investigated structurally related ROF-based membranes under mixed-gas and elevated-pressure conditions (3–10 bar) using an advanced gas permeation setup. The results of that research (Sandru et al., 2024) revealed stable $CO_2/CH_4$ selectivity trends under realistic conditions and confirmed the

robustness of ROF membranes up to 10 bar. These findings reinforce the current results and support the suitability of ROF membranes for applications such as biogas and landfill gas upgrading. Future research will focus on evaluating the long-term and high-pressure performance of the present ROF membranes under industrially relevant mixed-gas conditions.

## 4 Conclusion

In this study, we successfully constructed a new series of dynamic ROF membranes based on polyethylene oxide (PEO) segments for $CO_2/CH_4$ separation. By incorporating different lengths of PEO chains and adjusting the polymerization solvent (MeCN or NMP), we were able to fine-tune the membranes' architecture, control their crosslinking density, and influence the resulting microstructure. Spectroscopic and thermal analyses ($^1$H NMR, FTIR, TGA, and DSC) confirmed the successful synthesis of the ROF membranes and demonstrated their good thermal stability and partially hydrophobic surfaces.

As a result of these structural modifications, all fabricated membranes displayed balanced and tunable $CO_2$ transport properties. Increasing the length of the PEO segment led to enhanced dynamic mobility and pore accessibility within the membranes, promoting selective $CO_2$ permeation. This was further supported by the strong affinity between $CO_2$ and the polar functional groups present in the polymer backbone. Combined with the smaller kinetic diameter and higher quadrupole moment of $CO_2$, these structural features enabled a notable improvement in $CO_2$ permeability and $CO_2/CH_4$ selectivity.

The $CO_2/CH_4$ separation performance based on the Robeson upper-bound correlations showed that the membrane with the longest PEO segment achieved the most promising results, exceeding the 1991 Robeson limit and approaching the 2008 limit. Overall, this study highlights the effectiveness of tailoring the membrane architecture through segment length and solvent choice as a straightforward and versatile strategy for improving $CO_2/CH_4$ separation performance in PEO-based ROF membranes. These findings can serve as useful guideline for designing future ROF membranes with enhanced gas separation properties.

## Data availability statement

The raw data supporting the conclusions of this article will be made available by the authors without undue reservation.

## Author contributions

MY: Writing – original draft, Data curation, Investigation. LN: Writing – review and editing, Data curation, Methodology, Supervision, Investigation. LG: Writing – review and editing, Project administration, Supervision. JC: Formal Analysis, Conceptualization, Supervision, Methodology, Writing – review and editing. MB: Validation, Supervision, Conceptualization, Writing – review and editing, Investigation, Funding acquisition.

## Funding

The author(s) declare that financial support was received for the research and/or publication of this article. EUDIME Program (European Doctoral in Membrane Engineering) FCT/MCTES (LA/P/0008/2020 DOI 10.54499/LA/P/0008/2020, UIDP/50006/2020 DOI 10.54499/UIDP/50006/2020 and UIDB/50006/2020 DOI 10.54499/UIDB/50006/2020) "Evolution" funded by European Union—Nextgeneration EU and Romanian Government under the National Recovery and Resilience Plan for Romania, contract no.760033/23.05.2023 cod PNRR-C9-I8-CF16, through the Romanian Ministry of Research, Innovation and Digitalization, within Component 9, Investment I8.

## Conflict of interest

The authors declare that the research was conducted in the absence of any commercial or financial relationships that could be construed as a potential conflict of interest.

## Generative AI statement

The author(s) declare that no Generative AI was used in the creation of this manuscript.

Any alternative text (alt text) provided alongside figures in this article has been generated by Frontiers with the support of artificial intelligence and reasonable efforts have been made to ensure accuracy, including review by the authors wherever possible. If you identify any issues, please contact us.

## Publisher's note



## Supplementary material

The Supplementary Material for this article can be found online at: https://www.frontiersin.org/articles/10.3389/frmst.2025.1653220/full#supplementary-material

# References


Abdelrahim, M. Y. M., Osman, H. H., Cerneaux, S., Masquelez, N., and Barboiu, M. (2016). Extraction and membrane transport of lanthanides with dynameric constitutional framework carriers. *J. Membr. Sci.* 510, 50–57. doi:10.1016/j.memsci.2016.02.055

Abdelrahim, M. Y. M., Martins, C. F., Neves, L. A., Capasso, C., Supuran, C. T., Coelhoso, I. M., et al. (2017). Supported ionic liquid membranes immobilized with carbonic anhydrases for $CO_2$ transport at high temperatures. *J. Membr. Sci.* 528, 225–230. doi:10.1016/j.memsci.2017.01.033

Alexander Stern, S. (1994). Polymers for gas separations: the next decade. *J. Membr. Sci.* 94 (1), 1–65. doi:10.1016/0376-7388(94)00141-3

Aroon, M. A., Ismail, A. F., Matsuura, T., and Montazer-Rahmati, M. M. (2010). Performance studies of mixed matrix membranes for gas separation: a review. *Sep. Purif. Technol.* 75 (3), 229–242. doi:10.1016/j.seppur.2010.08.023

Azizi, N., Mohammadi, T., and Behbahani, R. M. (2017). Synthesis of a new nanocomposite membrane (PEBAX-1074/PEG-400/TiO2) in order to separate $CO_2$ from $CH_4$. *J. Nat. Gas Sci. Eng.* 37, 39–51. doi:10.1016/j.jngse.2016.11.038

Baker, R. W., and Low, B. T. (2014). Gas separation membrane materials: a perspective. *Macromolecules* 47 (20), 6999–7013. doi:10.1021/ma501488s

Bandehali, S., Moghadassi, A., Parvizian, F., Hosseini, S. M., Matsuura, T., and Joudaki, E. (2020). Advances in high carbon dioxide separation performance of poly (ethylene oxide)-based membranes. *J. Energy Chem.* 46, 30–52. doi:10.1016/j.jechem.2019.10.019

Bao, Z., Alnemrat, S., Yu, L., Vasiliev, I., Ren, Q., Lu, X., et al. (2011). Kinetic separation of carbon dioxide and methane on a copper metal–organic framework. *J. colloid interface Sci.* 357 (2), 504–509. doi:10.1016/j.jcis.2011.01.103

Barboiu, M. (2013). "Constitutional dynameric networks for membranes," in *Encyclopedia of membrane science and technology*, 1–18.

Basu, S., Khan, A. L., Cano-Odena, A., Liu, C., and Vankelecom, I. F. J. (2010). Membrane-based technologies for biogas separations. *Chem. Soc. Rev.* 39 (2), 750–768. doi:10.1039/B817050A

Basu, S., Cano-Odena, A., and Vankelecom, I. F. (2011). MOF-containing mixed-matrix membranes for $CO_2/CH_4$ and $CO_2/N_2$ binary gas mixture separations. *Sep. Purif. Technol.* 81 (1), 31–40. doi:10.1016/j.seppur.2011.06.037

Bengtson, G., Neumann, S., and Filiz, V. (2017). Membranes of polymers of intrinsic microporosity (PIM-1) modified by poly(ethylene glycol). *Membranes* 7 (2), 28. doi:10.3390/membranes7020028

Bondar, V., Freeman, B., and Pinnau, I. (2000). Gas transport properties of poly (ether-b-amide) segmented block copolymers. *J. Polym. Sci. Part B Polym. Phys.* 38 (15), 2051–2062. doi:10.1002/1099-0488(20000801)38:15<2051::aid-polb100>3.0.co;2-d

Brunetti, A., Scura, F., Barbieri, G., and Drioli, E. (2010). Membrane technologies for $CO_2$ separation. *J. Membr. Sci.* 359 (1), 115–125. doi:10.1016/j.memsci.2009.11.040

Budd, P. M., Msayib, K. J., Tattershall, C. E., Ghanem, B. S., Reynolds, K. J., McKeown, N. B., et al. (2005). Gas separation membranes from polymers of intrinsic microporosity. *J. Membr. Sci.* 251 (1), 263–269. doi:10.1016/j.memsci.2005.01.009

Car, A., Stropnik, C., Yave, W., and Peinemann, K. V. (2008). Tailor-made polymeric membranes based on segmented block copolymers for $CO_2$ separation. *Adv. Funct. Mater.* 18 (18), 2815–2823. doi:10.1002/adfm.200800436

Chatterjee, G., Houde, A., and Stern, S. (1997). Poly (ether urethane) and poly (ether urethane urea) membranes with high $H_2S/CH_4$ selectivity. *J. Membr. Sci.* 135 (1), 99–106. doi:10.1016/S0376-7388(97)00134-8

Chen, S., Zhou, T., Wu, H., Wu, Y., and Jiang, Z. (2017). Embedding molecular amine functionalized polydopamine submicroparticles into polymeric membrane for carbon capture. *Industrial and Eng. Chem. Res.* 56 (28), 8103–8110. doi:10.1021/acs.iecr.7b01546

Chuah, C. Y., Goh, K., Yang, Y., Gong, H., Li, W., Karahan, H. E., et al. (2018). Harnessing filler materials for enhancing biogas separation membranes. *Chem. Rev.* 118 (18), 8655–8769. doi:10.1021/acs.chemrev.8b00091

Comesaña-Gándara, B., Chen, J., Bezzu, C. G., Carta, M., Rose, I., Ferrari, M.-C., et al. (2019). Redefining the Robeson upper bounds for $CO_2/CH_4$ and $CO_2/N_2$ separations using a series of ultrapermeable benzotriptycene-based polymers of intrinsic microporosity. *Energy and Environ. Sci.* 12 (9), 2733–2740. doi:10.1039/C9EE01384A

Corrado, T., and Guo, R. (2020). Macromolecular design strategies toward tailoring free volume in glassy polymers for high performance gas separation membranes. *Mol. Syst. Des. and Eng.* 5 (1), 22–48. doi:10.1039/C9ME00099B

Cussler, E. L. (2009). *Diffusion: mass transfer in fluid systems*. United Kingom: Cambridge University Press.

D'Alessandro, D. M., Smit, B., and Long, J. R. (2010). Carbon dioxide capture: prospects for new materials. *Angew. Chem. Int. Ed.* 49 (35), 6058–6082. doi:10.1002/anie.201000431

Denny, M. S., Moreton, J. C., Benz, L., and Cohen, S. M. (2016). Metal–organic frameworks for membrane-based separations. *Nat. Rev. Mater.* 1 (12), 16078–17. doi:10.1038/natrevmats.2016.78

Dorosti, F., Omidkhah, M., and Abedini, R. (2014). Fabrication and characterization of Matrimid/MIL-53 mixed matrix membrane for $CO_2/CH_4$ separation. *Chem. Eng. Res. Des.* 92 (11), 2439–2448. doi:10.1016/j.cherd.2014.02.018

Dupuis, R., Barboiu, M., and Maurin, G. (2022). Unravelling the pore network and gas dynamics in highly adaptive rubbery organic frameworks. *Chem. Sci.* 13 (18), 5141–5147. doi:10.1039/D2SC01355J

Fares, M. M., Hacaloglu, J., and Suzer, S. (1994). Characterization of degradation products of polyethylene oxide by pyrolysis mass spectrometry. *Eur. Polym. J.* 30 (7), 845–850. doi:10.1016/0014-3057(94)90013-2

Freeman, B. D. (1999). Basis of permeability/selectivity tradeoff relations in polymeric gas separation membranes. *Macromolecules* 32 (2), 375–380. doi:10.1021/ma9814548

Ghadimi, A., Mohammadi, T., and Kasiri, N. (2014). A novel chemical surface modification for the fabrication of PEBA/$SiO_2$ nanocomposite membranes to separate $CO_2$ from syngas and natural gas streams. *Industrial and Eng. Chem. Res.* 53 (44), 17476–17486. doi:10.1021/ie503216p

Giovambattista, N., Debenedetti, P. G., and Rossky, P. J. (2007). Effect of surface polarity on water contact angle and interfacial hydration structure. *J. Phys. Chem. B* 111 (32), 9581–9587. doi:10.1021/jp071957s

Guo, A., Ban, Y., Yang, K., and Yang, W. (2018). Metal-organic framework-based mixed matrix membranes: synergetic effect of adsorption and diffusion for $CO_2/CH_4$ separation. *J. Membr. Sci.* 562, 76–84. doi:10.1016/j.memsci.2018.05.032

Herm, Z. R., Swisher, J. A., Smit, B., Krishna, R., and Long, J. R. (2011). Metal–organic frameworks as adsorbents for hydrogen purification and precombustion carbon dioxide capture. *J. Am. Chem. Soc.* 133 (15), 5664–5667. doi:10.1021/ja111411q

Ioannidi, A., Vroulias, D., Kallitsis, J., Ioannides, T., and Deimede, V. (2021). Synthesis and characterization of poly(ethylene oxide) based copolymer membranes for efficient gas/vapor separation: effect of PEO content and chain length. *J. Membr. Sci.* 632, 119353. doi:10.1016/j.memsci.2021.119353

Jia, M., Zhang, X.-F., Feng, Y., Zhou, Y., and Yao, J. (2020). *In-situ* growing ZIF-8 on cellulose nanofibers to form gas separation membrane for $CO_2$ separation. *J. Membr. Sci.* 595, 117579. doi:10.1016/j.memsci.2019.117579

Kang, C., Zhang, Z., Kusaka, S., Negita, K., Usadi, A. K., Calabro, D. C., et al. (2023). Covalent organic framework atropisomers with multiple gas-triggered structural flexibilities. *Nat. Mater.* 22 (5), 636–643. doi:10.1038/s41563-023-01523-2

Kawakami, M., Iwanaga, H., Hara, Y., Iwamoto, M., and Kagawa, S. (1982). Gas permeabilities of cellulose nitrate/poly (ethylene glycol) blend membranes. *J. Appl. Polym. Sci.* 27 (7), 2387–2393. doi:10.1002/app.1982.070270708

Kertik, A., Wee, L. H., Pfannmöller, M., Bals, S., Martens, J. A., and Vankelecom, I. F. J. (2017). Highly selective gas separation membrane using *in situ* amorphised metal–organic frameworks. *Energy and Environ. Sci.* 10 (11), 2342–2351. doi:10.1039/C7EE01872J

Kim, J. H., Ha, S. Y., and Lee, Y. M. (2001). Gas permeation of poly (amide-6-b-ethylene oxide) copolymer. *J. Membr. Sci.* 190 (2), 179–193. doi:10.1016/S0376-7388(01)00444-6

Koros, W. J., and Zhang, C. (2017). Materials for next-generation molecularly selective synthetic membranes. *Nat. Mater.* 16 (3), 289–297. doi:10.1038/nmat4805

Li, J., Nagai, K., Nakagawa, T., and Wang, S. (1995). Preparation of polyethyleneglycol (PEG) and cellulose acetate (CA) blend membranes and their gas permeabilities. *J. Appl. Polym. Sci.* 58 (9), 1455–1463. doi:10.1002/app.1995.070580906

Lin, H., and Freeman, B. D. (2004). Gas solubility, diffusivity and permeability in poly (ethylene oxide). *J. Membr. Sci.* 239 (1), 105–117. doi:10.1016/j.memsci.2003.08.031

Lin, H., Van Wagner, E., Raharjo, R., Freeman, B. D., and Roman, I. (2006a). High-performance polymer membranes for natural-gas sweetening. *Adv. Mater.* 18 (1), 39–44. doi:10.1002/adma.200501409

Lin, H., Wagner, E. V., Swinnea, J. S., Freeman, B. D., Pas, S. J., Hill, A. J., et al. (2006b). Transport and structural characteristics of crosslinked poly(ethylene oxide) rubbers. *J. Membr. Sci.* 276 (1), 145–161. doi:10.1016/j.memsci.2005.09.040

Luo, S., Stevens, K. A., Park, J. S., Moon, J. D., Liu, Q., Freeman, B. D., et al. (2016). Highly $CO_2$-selective gas separation membranes based on segmented copolymers of poly(ethylene oxide) reinforced with pentiptycene-containing polyimide hard segments. *ACS Appl. Mater. and Interfaces* 8 (3), 2306–2317. doi:10.1021/acsami.5b11355

McKeown, N. B. (2020). Polymers of intrinsic microporosity (PIMs). *Polymer* 202, 122736. doi:10.1016/j.polymer.2020.122736

Moghadassi, A. R., Rajabi, Z., Hosseini, S. M., and Mohammadi, M. (2014). Fabrication and modification of cellulose acetate based mixed matrix membrane: gas separation and physical properties. *J. Industrial Eng. Chem.* 20 (3), 1050–1060. doi:10.1016/j.jiec.2013.06.042

Mubashir, M., Yeong, Y. F., Lau, K. K., Chew, T. L., and Norwahyu, J. (2018). Efficient $CO_2/N_2$ and $CO_2/CH_4$ separation using $NH_2$-MIL-53(Al)/cellulose acetate (CA) mixed matrix membranes. *Sep. Purif. Technol.* 199, 140–151. doi:10.1016/j.seppur.2018.01.038

Mubashir, M., Yeong, Y. F., Lau, K. K., and Chew, T. L. (2019). Effect of spinning conditions on the fabrication of cellulose acetate hollow fiber membrane for $CO_2$ separation from $N_2$ and $CH_4$. *Polym. Test.* 73, 1–11. doi:10.1016/j.polymertesting.2018.10.036

Nasr, G., Barboiu, M., Ono, T., Fujii, S., and Lehn, J.-M. (2008). Dynamic polymer membranes displaying tunable transport properties on constitutional exchange. *J. Membr. Sci.* 321 (1), 8–14. doi:10.1016/j.memsci.2008.03.005

Nasr, G., Macron, T., Gilles, A., Petit, E., and Barboiu, M. (2012). Systems membranes–combining the supramolecular and dynamic covalent polymers for gas-selective dynameric membranes. *Chem. Commun.* 48 (59), 7398–7400. doi:10.1039/C2CC33603K

Nebipasagil, A., Park, J., Lane, O. R., Sundell, B. J., Mecham, S. J., Freeman, B. D., et al. (2017). Polyurethanes containing Poly(arylene ether sulfone) and Poly(ethylene oxide) segments for gas separation membranes. *Polymer* 118, 256–267. doi:10.1016/j.polymer.2017.03.017

Neves, L. A., Afonso, C., Coelhoso, I. M., and Crespo, J. G. (2012). Integrated $CO_2$ capture and enzymatic bioconversion in supported ionic liquid membranes. *Sep. Purif. Technol.* 97, 34–41. doi:10.1016/j.seppur.2012.01.049

Nordin, N. A. H. M., Ismail, A. F., Mustafa, A., Murali, R. S., and Matsuura, T. (2015). Utilizing low ZIF-8 loading for an asymmetric PSf/ZIF-8 mixed matrix membrane for $CO_2/CH_4$ separation. *RSC Adv.* 5 (38), 30206–30215. doi:10.1039/C5RA00567A

Okamoto, K.-i., Fuji, M., Okamyo, S., Suzuki, H., Tanaka, K., and Kita, H. (1995). Gas permeation properties of poly (ether imide) segmented copolymers. *Macromolecules* 28 (20), 6950–6956. doi:10.1021/ma00124a035

Patel, N. P., Miller, A. C., and Spontak, R. J. (2004). Highly $CO_2$-permeable and -selective membranes derived from crosslinked poly(ethylene glycol) and its nanocomposites. *Adv. Mater.* 14 (7), 699–707. doi:10.1002/adfm.200305136

Petzetakis, N., Doherty, C. M., Thornton, A. W., Chen, X. C., Cotanda, P., Hill, A. J., et al. (2015). Membranes with artificial free-volume for biofuel production. *Nat. Commun.* 6 (1), 7529–8. doi:10.1038/ncomms8529

Pourafshari Chenar, M., Soltanieh, M., Matsuura, T., Tabe-Mohammadi, A., and Khulbe, K. C. (2006). The effect of water vapor on the performance of commercial polyphenylene oxide and Cardo-type polyimide hollow fiber membranes in $CO_2/CH_4$ separation applications. *J. Membr. Sci.* 285 (1), 265–271. doi:10.1016/j.memsci.2006.08.028

Qiu, Y., Ren, J., Zhao, D., Li, H., and Deng, M. (2016). Poly(amide-6-b-ethylene oxide)/[Bmim] [$Tf_2N$] blend membranes for carbon dioxide separation. *J. Energy Chem.* 25 (1), 122–130. doi:10.1016/j.jechem.2015.10.009

Rahman, M. M., Filiz, V., Shishatskiy, S., Abetz, C., Neumann, S., Bolmer, S., et al. (2013). PEBAX® with PEG functionalized POSS as nanocomposite membranes for $CO_2$ separation. *J. Membr. Sci.* 437, 286–297. doi:10.1016/j.memsci.2013.03.001

Refaat, D., Yahia, M., and Coronas, J. (2024). Thin film nanocomposite membranes based on renewable polymer Pebax® and zeolitic imidazolate frameworks for $CO_2/CH_4$ separation. *Process Saf. Environ. Prot.* 192, 401–411. doi:10.1016/j.psep.2024.10.053

Reijerkerk, S. R., Knoef, M. H., Nijmeijer, K., and Wessling, M. (2010). Poly(ethylene glycol) and poly(dimethyl siloxane): combining their advantages into efficient $CO_2$ gas separation membranes. *J. Membr. Sci.* 352 (1), 126–135. doi:10.1016/j.memsci.2010.02.008

Robeson, L. M. (1991). Correlation of separation factor versus permeability for polymeric membranes. *J. Membr. Sci.* 62 (2), 165–185. doi:10.1016/0376-7388(91)80060-J

Robeson, L. M. (2008). The upper bound revisited. *J. Membr. Sci.* 320 (1-2), 390–400. doi:10.1016/j.memsci.2008.04.030

Robeson, L. M., Freeman, B. D., Paul, D. R., and Rowe, B. W. (2009). An empirical correlation of gas permeability and permselectivity in polymers and its theoretical basis. *J. Membr. Sci.* 341 (1), 178–185. doi:10.1016/j.memsci.2009.06.005

Rowe, B. W., Robeson, L. M., Freeman, B. D., and Paul, D. R. (2010). Influence of temperature on the upper bound: theoretical considerations and comparison with experimental results. *J. Membr. Sci.* 360 (1-2), 58–69. doi:10.1016/j.memsci.2010.04.047

Roy, N., Bruchmann, B., and Lehn, J.-M. (2015). DYNAMERS: dynamic polymers as self-healing materials. *Chem. Soc. Rev.* 44 (11), 3786–3807. doi:10.1039/C5CS00194C

Sanaeepur, H., Kargari, A., Nasernejad, B., Ebadi Amooghin, A., and Omidkhah, M. (2016). A novel $Co^{2+}$ exchanged zeolite Y/cellulose acetate mixed matrix membrane for $CO_2/N_2$ separation. *J. Taiwan Inst. Chem. Eng.* 60, 403–413. doi:10.1016/j.jtice.2015.10.042

Sanchez, J., Charmette, C., and Gramain, P. (2002). Poly (ethylene oxide-co-epichlorohydrin) membranes for carbon dioxide separation. *J. Membr. Sci.* 205 (1-2), 259–263. doi:10.1016/S0376-7388(02)00124-2

Sandru, M., Prache, M., Macron, T., Căta, L., Ahunbay, M. G., Hägg, M.-B., et al. (2024). Rubbery organic frameworks (ROFs) toward ultrapermeable $CO_2$-selective membranes. *Sci. Adv.* 10 (46), eadq5024. doi:10.1126/sciadv.adq5024

Sheng, L., Guo, Y., Zhao, D., Ren, J., Wang, S., and Deng, M. (2020). Enhanced $CO_2/CH_4$ separation performance of BTDA-TDI/MDI (P84) copolyimide mixed-matrix membranes by incorporating submicrometer-sized [$Ni_3(HCOO)_6$] framework crystals. *J. Nat. Gas Sci. Eng.* 75, 103123. doi:10.1016/j.jngse.2019.103123

Sridhar, S., Smitha, B., and Aminabhavi, T. M. (2007). Separation of carbon dioxide from natural gas mixtures through polymeric membranes—a review. *Sep. and Purif. Rev.* 36 (2), 113–174. doi:10.1080/15422110601165967

Staudt-Bickel, C., and Koros, J. (1999). Improvement of $CO_2/CH_4$ separation characteristics of polyimides by chemical crosslinking. *J. Membr. Sci.* 155 (1), 145–154. doi:10.1016/S0376-7388(98)00306-8

Suzuki, H., Tanaka, K., Kita, H., Okamoto, K., Hoshino, H., Yoshinaga, T., et al. (1998). Preparation of composite hollow fiber membranes of poly (ethylene oxide)-containing polyimide and their $CO_2/N_2$ separation properties. *J. Membr. Sci.* 146 (1), 31–37. doi:10.1016/S0376-7388(98)00081-7

Swaidan, R., Ghanem, B., and Pinnau, I. (2015). Fine-tuned intrinsically ultramicroporous polymers redefine the permeability/selectivity upper bounds of membrane-based air and hydrogen separations. *ACS Macro Lett.* 4 (9), 947–951. doi:10.1021/acsmacrolett.5b00512

Tena, A., Marcos-Fernández, A., Palacio, L., Prádanos, P., Lozano, A. E., de Abajo, J., et al. (2013). On the influence of the proportion of PEO in thermally controlled phase segregation of copoly(ether-imide)s for gas separation. *J. Membr. Sci.* 434, 26–34. doi:10.1016/j.memsci.2013.01.036

Theodosopoulos, G. V., Zisis, C., Charalambidis, G., Nikolaou, V., Coutsolelos, A. G., and Pitsikalis, M. (2017). Synthesis, characterization and thermal properties of poly(ethylene oxide), PEO, polymacromonomers via anionic and ring opening metathesis polymerization. *Polymers* 9 (4), 145. doi:10.3390/polym9040145

Vöge, A., Deimede, V., and Kallitsis, J. K. (2014a). Synthesis and properties of alkaline stable pyridinium containing anion exchange membranes. *RSC Adv.* 4 (85), 45040–45049. doi:10.1039/C4RA07616H

Vöge, A., Deimede, V., Paloukis, F., Neophytides, S. G., and Kallitsis, J. K. (2014b). Synthesis and properties of aromatic polyethers containing poly (ethylene oxide) side chains as polymer electrolytes for lithium ion batteries. *Mater. Chem. Phys.* 148 (1-2), 57–66. doi:10.1016/j.matchemphys.2014.07.012

Vollas, A., Chouliaras, T., Deimede, V., Ioannides, T., and Kallitsis, J. (2018). New pyridinium type poly(ionic liquids) as membranes for $CO_2$ separation. *Polymers* 10 (8), 912. doi:10.3390/polym10080912

Wang, S., Li, X., Wu, H., Tian, Z., Xin, Q., He, G., et al. (2016). Advances in high permeability polymer-based membrane materials for $CO_2$ separations. *Energy and Environ. Sci.* 9 (6), 1863–1890. doi:10.1039/C6EE00811A

Xing, R., and Ho, W. S. W. (2009). Synthesis and characterization of crosslinked polyvinylalcohol/polyethyleneglycol blend membranes for $CO_2/CH_4$ separation. *J. Taiwan Inst. Chem. Eng.* 40 (6), 654–662. doi:10.1016/j.jtice.2009.05.004

Yahia, M., Lozano, L. A., Zamaro, J. M., Téllez, C., and Coronas, J. (2024). Microwave-assisted synthesis of metal–organic frameworks UiO-66 and MOF-808 for enhanced $CO_2/CH_4$ separation in PIM-1 mixed matrix membranes. *Sep. Purif. Technol.* 330, 125558. doi:10.1016/j.seppur.2023.125558

Yahia, M., Refaat, D., Coronas, J., and Tellez, C. (2025). Enhancing $CO_2/CH_4$ separation performance in PIM-1 based MXene nanosheets mixed matrix membranes. *Sep. Purif. Technol.* 356, 129825. doi:10.1016/j.seppur.2024.129825

Yave, W., Car, A., Funari, S. S., Nunes, S. P., and Peinemann, K.-V. (2010). $CO_2$-Philic polymer membrane with extremely high separation performance. *Macromolecules* 43 (1), 326–333. doi:10.1021/ma901950u

Yoshino, M., Ito, K., Kita, H., and Okamoto, K. I. (2000). Effects of hard-segment polymers on $CO_2/N_2$ gas-separation properties of poly (ethylene oxide)-segmented copolymers. *J. Polym. Sci. Part B Polym. Phys.* 38 (13), 1707–1715. doi:10.1002/1099-0488(20000701)38:13<1707::aid-polb40>3.3.co;2-n

Zhang, Y., and Barboiu, M. (2016). Constitutional dynamic materials toward natural selection of function. *Chem. Rev.* 116 (3), 809–834. doi:10.1021/acs.chemrev.5b00168

Zou, X., and Zhu, G. (2018). Microporous organic materials for membrane-based gas separation. *Adv. Mater.* 30 (3), 1700750. doi:10.1002/adma.201700750